Published in final edited form as:
Mol Imaging Biol. 2012 February ; 14(1): 70–78. doi:10.1007/s11307-011-0476-4.

Positron Emission Tomography of Copper Metabolism in the *Atp7b*$^{-/-}$ Knock-out Mouse Model of Wilson's Disease

Fangyu Peng[1,2,3], **Svetlana Lutsenko**[4], **Xiankai Sun**[1,2], and **Otto Muzik**[5,6]

[1] Department of Radiology, University of Texas Southwestern Medical Center, 5323 Harry Hines Blvd, Dallas, TX, 75390-8542, USA

[2] Advanced Imaging Research Center, University of Texas Southwestern Medical Center, Dallas, TX, USA

[3] Harold C. Simmons Comprehensive Cancer Center, University of Texas Southwestern Medical Center, Dallas, TX, USA

[4] Department of Physiology, Johns Hopkins University, Baltimore, MD, USA

[5] Carman & Ann Adams Department of Pediatrics, School of Medicine, Wayne State University, Detroit, MI, USA

[6] Department of Radiology, School of Medicine, Wayne State University, Detroit, MI, USA

Abstract

Purpose—This study aims to determine feasibility and utility of copper-64(II) chloride ($^{64}CuCl_2$) as a tracer for positron emission tomography (PET) of copper metabolism imbalance in human Wilson's disease (WD).

Procedures—*Atp7b*$^{-/-}$ mice, a mouse model of human WD, were injected with $^{64}CuCl_2$ intravenously and subjected to PET scanning using a hybrid PET-CT (computerized tomography) scanner, with the wild-type C57BL mice as a normal control. Quantitative PET analysis was performed to determine biodistribution of ^{64}Cu radioactivity and radiation dosimetry estimates of ^{64}Cu were calculated for PET of copper metabolism in humans.

Results—Dynamic PET analysis revealed increased accumulation and markedly reduced clearance of ^{64}Cu from the liver of the *Atp7b*$^{-/-}$ mice, compared to hepatic uptake and clearance of ^{64}Cu in the wild-type C57BL mice. Kinetics of copper clearance and retention was also altered for kidneys, heart, and lungs in the *Atp7b*$^{-/-}$ mice. Based on biodistribution of ^{64}Cu in wild-type C57BL mice, radiation dosimetry estimates of ^{64}Cu in normal human subjects were obtained, showing an effective dose (ED) of 32.2 μ (micro)Sv/MBq (weighted dose over 22 organs) and the small intestine as the critical organ for radiation dose (61 μGy/MBq for males and 69 μGy/MBq for females). Radiation dosimetry estimates for the patients with WD, based on biodistribution of ^{64}Cu in the *Atp7b*$^{-/-}$ mice, showed a similar ED of 32.8 μ (micro)Sv/MBq (p= 0.53), with the liver as the critical organ for radiation dose (120 μSv/MBq for male and 161 μSv/MBq for female).

Conclusions—Quantitative PET analysis demonstrates abnormal copper metabolism in the mouse model of WD with improved time–resolution. Human radiation dosimetry estimates obtained in this preclinical study encourage direct radiation dosimetry of $^{64}CuCl_2$ in human

Correspondence to: Fangyu Peng; Fangyu.Peng@UTSouthwestern.edu.

The authors declare that they have no conflict of interest.

subjects. The results suggest feasibility of utilizing $^{64}CuCl_2$ as a tracer for noninvasive assessment of copper metabolism in WD with PET.

Keywords

Copper metabolism; Wilson's disease; *ATP7B* copper transporter; Positron emission tomography; Copper-64 (II) chloride; Radiation dosimetry

Introduction

Copper metabolism is an important physiological process in humans. Copper is an essential element, which is required for normal function of numerous key metabolic enzymes, however in excess copper is toxic [1, 2]. Absorption, distribution, and clearance of copper are tightly regulated [3, 4] by a finely-tuned network of copper transporters [5, 6]. In humans, malfunction of copper transporters causes disruption of copper homeostasis and severe disorders [7] which include WD caused by a mutation of the *ATP7B* (ATPase, Cu +transporting, beta polypeptide) gene [8, 9] and Menkes disease caused by a mutation of the *ATP7A* (ATPase, Cu+transporting, α polypeptide) gene [10–12]. WD is an autosomal-recessive disorder with a birth incidence rate of approximately 1:30,000 and about 1% of population being carriers of *ATP7B* gene mutation [13]. Accumulating evidence suggests that the imbalance of copper metabolism also significantly contributes to the pathogenesis of such human diseases as Alzheimer's disease [14], cancer [15], and cardiovascular disease [16].

Mechanistic understanding of the role of copper in pathophysiology of human diseases requires a non-invasive assessment of copper metabolism *in vivo.* Previously, radioactive copper was used to study copper absorption and distribution in rodents by counting radioactivity of body fluids or tissues *ex vivo* [17–19]. These studies have yielded useful information about copper distribution between tissues, but real-time copper fluxes *in vivo* remain largely uncharacterized. Kinetics of copper uptake and clearance may vary greatly between different organs and may inform on disease onset and progression. Thus, in recent years, there has been a considerable interest in developing quantitative approaches to measure copper *in vivo* [20–23].

Chemical indicators and probes in conjunction with microscopic examination have been employed for studying copper status in cells, but they are not yet suitable for direct analysis of copper flow in living animals or humans. Chemical agents for magnetic resonance imaging (MRI) [20, 21] are useful for static quantification of copper ions in animal organs or tissues, but may have low sensitivity for tracking flow of a trace amount of copper *in vivo*. The application of promising fluorescent tracers [22, 23] for the analysis of copper flow in live organisms needs to overcome limited tissue penetration, high background fluorescence, and quenching of fluorescence signals. To enable accurate understanding of copper physiology and clinical applications, it is necessary to search for additional imaging agents allowing quantitative and longitudinal analysis of copper flow *in vivo*, particularly noninvasive assessment of copper metabolism in humans.

Positron emission tomography (PET) is a highly sensitive and quantitative molecular imaging technology, which is particularly well suited for systemic analysis of copper metabolism in animals and humans. Several positron-emitting copper isotopes are currently available [24] which include ^{62}Cu ($t_{1/2}$ 9.74 m, 98% β+) and ^{64}Cu ($t_{1/2}$ 12.7 h, 17% β+). The goal of this study was to determine feasibility of using $^{64}CuCl_2$ as a tracer for noninvasive assessment of copper metabolism imbalance in WD with PET. To reach this goal, we utilized *Atp7b*$^{-/-}$ mice, an established animal model for WD. Specifically, we aimed: (1) to

determine biodistribution of ^{64}Cu in *Atp7b*$^{-/-}$ mice injected with $^{64}CuCl_2$ intravenously, in comparison with the control C57BL mice; and (2) based on biodistribution in mice, obtain ^{64}Cu radiation dosimetry estimates for PET of copper metabolism in humans. By performing dynamic PET, we obtained the first real-time measurements of ^{64}Cu distribution in the organs or tissues of *Atp7b*$^{-/-}$ mice. The human radiation dosimetry estimates of ^{64}Cu were also calculated, which encourage direct radiation dosimetry and PET of copper metabolism in the patients with WD using $^{64}CuCl_2$ as a tracer.

Materials and methods

Animals and radiopharmaceuticals

The *Atp7b*$^{-/-}$ mice (5–6 weeks old, *N*=4, two male and two female) and the control wild-type C57BL mice (12–13 weeks old, *N*=4, two male and two female) were transferred from Johns Hopkins University (Baltimore, MD, USA) to UT Southwestern Medical Center (Dallas, TX, USA) and used for this study at the age of 7–8 weeks (*Atp7b*$^{-/-}$) or 15–16 weeks old (C57BL mice). Copper-64 produced via $^{64}Ni(p,n)^{64}Cu$ on a biomedical cyclotron was purchased from Washington University (St Louis, MO, USA) in the form of $^{64}CuCl_2$ in 0.1 N HCl solution. The specific activity of ^{64}Cu was around 6.9±2.5 Ci/μmol.

Animal PET-CT

All animal experiments were conducted under the protocol approved by the UT Southwestern Institutional Animal Care and Use Committee. PET of mice was performed with a Siemens Inveon PET/computerized tomography (CT) Multimodality System, using a protocol modified from those described previously [25, 26]. Calibration of the PET/CT scanner was performed with an in-house manufactured phantom containing a dose of $^{64}CuCl_2$ as a radiation source. Briefly, mice were anesthetized using 3% isoflurane at room temperature and placed in spread–supine position on the imaging bed under 2% isoflurane anesthesia for the duration of the imaging. Initially, a helical CT scan was acquired (80 kV, 500 μA) with a pixel size of ~0.1 mm in order to create an anatomical image that was subsequently used for attenuation correction of the PET emission data. Following conclusion of the CT scan, mice were injected with the tracer $^{64}CuCl_2$ (74 kBq or 2 μCi/g body weight), diluted with normal saline containing 0.9% sodium chloride into a total volume of 100 μL intravenously via the tail vein. Immediately after administration of the tracer, dynamic whole body data acquisition was started for 1 h with the liver in the center of the field of view. In addition, static whole body imaging was performed at 2 and 24 h post injection of the tracer, which consisted of two overlapping frames of 15 min duration for each frame. PET images were reconstructed using the ordered subsets expectation maximization 3D algorithm and analyzed using the Inveon Research Workplace software (Siemens) which allows fusion of CT and PET image volumes, the re-slicing of fused images into arbitrary views and the definition of regions of interests (ROIs) in order to obtain time-activity curves that were further processed as described below.

Dosimetry calculation for ^{64}Cu radioactivity

ROIs for various organs were defined on serial axial images and non-decay corrected time–activity curves were obtained for the following organs: brain, heart, lung, liver, kidneys, bladder, small intestine, upper large intestine, lower large intestine, testis, muscle, and blood (blood pool of large blood vessels in the superior mediastinum). Time–activity curves were extended to 24 h by combining the initial dynamic scan with scans obtained at 2 and 24 h post injection. The residence time for each organ was then calculated as the integral under the time–activity curve normalized to the injected activity and multiplying the result with the weight of the organ. The absorbed dose to the organs was calculated assuming homogeneous distribution of the activity throughout the organ. The residence time of the remainder

activity was accounted for by subtracting the residence time determined for the organs from the inverse of the decay constant for ^{64}Cu (18.3 h^{-1}). Since blood is not a source organ of medical internal radionuclide dose, blood activity was assigned to the remainder of the body. Subsequently, these residence times were used together with the OLINDA software [27, 28] in order to estimate the dose to multiple organs. The OLINDA software considers all doses from a source to a specific target organ contributed by the various decay schemes of ^{64}Cu (β+, β−, EC, and *r*) and yields the effective dose (ED), which is representative of the overall radiation dose to a subject from PET imaging.

Statistical analysis

In order to assess significant differences in ^{64}Cu biodistribution between *Atp7b*$^{-/-}$ and C57BL wild-type mice, a 2×(8) mixed-design analysis was conducted, where the between-subjects factor represents the group (*Atp7b*$^{-/-}$, C57BL mice) and the within-subjects factor represents the radiation dose in regions that showed either the highest ^{64}Cu radioactivity or regions known to be most sensitive to radiation (liver, kidney, small intestines, upper large bowel, lower large bowel, lungs, heart, gonads). The overall test was subsequently followed up by post-hoc unpaired *t* tests between the two groups for individual regions. Finally, we applied an unpaired *t* test in order to determine whether there are significant differences in the calculated ED values between males and females with WD and control subjects. A *p* value <0.05 was considered to represent statistical significance.

Results

Increased uptake and accumulation of ^{64}Cu in the liver of Atp7b$^{-/-}$ mice

Copper metabolism in the liver is regulated by a single copper-transporting ATPase *Atp7b*, whereas in most of the other tissues two Cu-ATPases, *Atp7a and Atp7b* work together to maintain copper balance. In normal liver, the function of *Atp7b* is to transport copper into the secretory pathway for incorporation into ceruloplasmin and to export excess copper into the bile. Consequently, in *Atp7b*$^{-/-}$ mice, we expected to observe poor copper excretion from the liver due to *Atp7b* inactivation leading to higher levels of hepatic copper. Based on earlier work with WD patients [29, 30], the uptake of copper into the *Atp7b*$^{-/-}$ liver was also expected to be elevated, although the mechanism behind this increase remains unknown. Since the time-resolved quantitative analysis of copper uptake has never been done in live *Atp7b*$^{-/-}$ mice, we performed measurements of ^{64}Cu accumulation using dynamic PET imaging in order to assess the kinetics of copper uptake in a pre-clinically relevant time frame.

Whole body images from dynamic imaging at 0–1 h post-injection showed intense ^{64}Cu radioactivity in the liver and much lower intensity in other organs or tissues, for both the control C57BL and the *Atp7b*$^{-/-}$ mice (Fig. 1). There was a continued accumulation of ^{64}Cu in the liver of *Atp7b*$^{-/-}$ mice, whereas initial rapid uptake of ^{64}Cu in the liver of the control C57BL mice was followed by a gradual clearance of the tracer from the liver to the intestines via hepatobilliary clearance pathway. Static whole body images at 24 h post-injection showed much higher ^{64}Cu radioactivity in the liver of the *Atp7b*$^{-/-}$ mice than control C57BL mice (Fig. 1). Time-activity curves demonstrated that the initial rate of hepatic copper uptake was significantly higher in *Atp7b*$^{-/-}$ mice compared to control (Fig. 2). The continuing copper accumulation resulted in a marked difference of hepatic ^{64}Cu radioactivity between the *Atp7b*$^{-/-}$ and control C57BL mice at 24 h post-injection. The percentage of injected dose per gram %ID/g of hepatic ^{64}Cu uptake was significantly higher in *Atp7b*$^{-/-}$ mice as compared to C57BL mice (52.3±6.6 vs. 10.9±1.7, $p<0.001$; Fig. 3).

Renal uptake and clearance of ^{64}Cu in the Atp7b$^{-/-}$ mice

Among extrahepatic organs, kidneys have a relatively high level of *Atp7b* but also express *Atp7a*. Consequently, we studied whether the loss of *Atp7b* was associated with a rapid copper accumulation and reduced clearance similar to that observed in the liver. Our measurements revealed that this was not the case. Renal uptake of ^{64}Cu in the *Atp7b*$^{-/-}$ in the initial 60 min was similar to those of the control C57BL mice (Fig. 2), with the ^{64}Cu radioactivity gradually decreasing in both animal strains. At 24 post-injection of the tracer, the renal %ID/g of ^{64}Cu was significantly lower in the *Atp7b*$^{-/-}$ mice as compared to controls (1.93±0.67 vs. 4.08± 0.86, p=0.01, Fig. 3). There was no simultaneous increase of ^{64}Cu radioactivity in the urinary bladder, and the amount of ^{64}Cu radioactivity in the urinary bladder was low, indicative of the lack of significant copper excretion via this route.

^{64}Cu distribution in other tissues of Atp7b$^{-/-}$ mice

^{64}Cu radioactivity in several other organs of *Atp7b*$^{-/-}$ mice was lower than that determined in control C57BL mice (Fig. 3) at 24 h post-injection, which was independent of some initial differences in the distribution kinetics. For example, in the first hour post-injection of the tracer, Cu^{64} radioactivity in both the heart and lungs of *Atp7b*$^{-/-}$ mice was higher than those in C57BL mice. However, at 24 h post-injection, the %ID/g of ^{64}Cu in the heart of *Atp7b*$^{-/-}$ mice was significantly lower than those in the C57BL mice (1.11±0.50 vs. 2.42±0.67, p=0.02), but similar for the lungs (2.06±0.62 vs. 2.64±0.34, p=0.15; Fig. 3). Finally, quantitative analysis revealed consistently lower ^{64}Cu radioactivity at all times in the brain of *Atp7b*$^{-/-}$ mice as compared to C57BL mice, which was significant at 24 h post-injection (0.28+0.05 vs. 0.63+0.17, p<0.01).

Radiation dosimetry estimates of $^{64}CuCl_2$ in humans

The residence times (see Table 1) were calculated from kinetic ^{64}Cu PET data in C57BL wild-type and *Atp7b*$^{-/-}$ mice. Based on these residence times, organ-absorbed radiation dose estimates in humans were calculated as shown in Table 2. The results indicate that, whereas in control subjects the critical organ is the small intestine (61 μGy/MBq for males and 69 μGy/MBq for females), in patients with WD the critical organ is the liver (120 and 161 μGy/MBq for males and females, respectively, Fig. 4). Application of a mixed-design ANOVA showed a significantly higher absorbed dose only for the liver (p=0.003) in patients with WD. Administration of 5 MBq/kg (0.14 mCi/kg) of $^{64}CuCl_2$ for PET studies results in a total PET dose of 9.4±0.96 mSv in the control group and a similar dose of 10.1+10.04 mSv in patients with WD (p=0.53, Table 3). Figure 5 shows the total PET dose for both genders and the two groups under study. Finally, the effective dose originating from PET imaging using $^{64}CuCl_2$ was only 20% higher than that determined in 2-deoxy-2-[^{18}F]fluoro-D-glucose ([^{18}F]FDG studies; 32 vs. 27 μSv/MBq) [31]. Moreover, the average dose to the critical organ (small intestines for control subjects or liver for patients with WD) is about half (63 μSv/MBq and 140 μSv/MBq, respectively) of that compared with the critical organ for [^{18}F]FDG, which is the urinary bladder (220 μSv/MBq). Thus, the overall radiation dose for a PET study using $^{64}CuCl_2$ is comparable to that for the established [^{18}F]FDG PET.

Discussion

Systemic analysis of whole body copper metabolism is important for understanding of molecular mechanisms that maintain copper homeostasis in humans. In particular, identifying temporal and spatial differences in copper distribution is needed in order to elucidate the pathophysiology of copper misbalance in diseases such as WD [6, 7]. In recent years, significant progress has been made in characterization of cellular machinery that controls copper homeostasis; however, little is known about real-time copper distribution between tissues in either normal person or in the patients with copper-related disorders.

Previously, attempts were made to assess copper metabolism in the patients diagnosed with WD using a nuclear scanner and ^{64}Cu or ^{67}Cu isotopes [29, 30, 32, 33] and in Long–Evans cinnamon rats, a rat model of WD with a microPET scanner [34]. In the 1960s, Osborn et al. [29] conducted abdominal scintiscans in 27 patients with WD (six in the presymptomatic, six in the hepatic, and 15 in the neurological stages of the disease) using a Picker Magnascanner. The patients were injected with 0.2–0.6 mCi of $^{64}CuCl_2$ in normal saline as a single intravenous injection following withdrawal of blood into the syringe to ensure adequate mixing with plasma proteins before injection. It was found that the hepatic concentrating power for copper decreased along with progression of the disease and the extrahepatic (presumably renal) deposits of radioactivity become more conspicuous and the general tissue level of radioactivity increase. However, limited spatial resolution of the scintiscanner available at that time did not allow more detailed and quantitative analysis of copper radioactivity at various tissues and organs. Radiation dosimetry of $^{64}CuCl_2$ or $^{67}CuCl_2$ was not reported in the literature, most likely because the limited spatial resolution of the instruments used in the previous studies prevented measurements of the radioactive copper concentration in specific organs or tissues. Improved spatial resolution of a modern animal PET/CT scanner made it possible to conduct preclinical radiation dosimetry based on biodistribution of ^{64}Cu radioactivity in animals prior to direct radiation dosimetry in human subjects.

Recent advances in hybrid PET-CT, as well as hybrid PET-MRI are expected to invigorate interest in utilization of PET for study of copper metabolism *in vivo*. PET/CT is particularly suitable for non-invasive assessment of whole body copper metabolism, but the lack of a tracer approved for use in humans has hampered application of PET for mechanistic investigations of molecular mechanisms of copper misbalance in human diseases. In the clinic, the high sensitivity of PET combined with superior spatial resolution of CT and MRI [35, 36] make it ideal for noninvasive, time-dependant analysis of copper metabolism in humans.

To develop a tracer for PET of copper metabolism in humans, we assessed copper distribution in *Atp7b*$^{-/-}$ mice, an established mouse model of WD [37], using a state of the art animal PET-CT scanner (Siemens Inveon PET/CT Multimodality System). High spatial resolution of the PET-CT scanner allowed for the first time kinetic analysis of copper distribution in various organs or tissues in living animals, thus improving upon the earlier studies where only radioactive copper flow to the liver could have been reliably assessed. As expected, rapid uptake and accumulation of copper was found in the liver of *Atp7b*$^{-/-}$ mice in association with dramatically reduced hepatobilliary clearance compared with that in wild-type C57BL mice, as visualized on the PET-CT images (Fig. 1) and time–activity curves (Fig. 2). Consistent with the early reports in presymptomatic WD patients, the 6-week-old *Atp7b*$^{-/-}$ mice show increased kinetics of hepatic copper uptake, thus further validating this mouse model of WD. Although the *Atp7b*$^{-/-}$ mice used in this study were younger than the control wild-type C57BL mice (5–6 weeks old versus 12–13 weeks old), we do not expect significant difference of copper metabolism in the wild-type C57BL mice aged 5–6 or 12–13 weeks old based on our observation from other experiments.

In contrast to the liver, ^{64}Cu radioactivity from extra-hepatic tissues, including brain, kidneys, lungs, and heart, is significantly lower in the *Atp7b*$^{-/-}$ mice compared to control C57BL mice (Figs. 2 and 3). The reduced ^{64}Cu radioactivity in the *Atp7b*$^{-/-}$ extrahepatic tissues may be caused by hepatic sequestration. Since copper taken by the liver is normally transported by *Atp7b*$^{-/-}$ to ceruloplasmin and other copper-containing proteins in the secretory pathway; the diminished copper uptake by extrahepatic tissues implies the role for such cupro-proteins in bioavailability of copper to these tissues. The role for cupro-proteins in copper delivery to extrahepatic tissues was earlier suggested in the experiments with rats

[38], but remained controversial due to the lack of marked changes in copper metabolism in cerulo-plasmin-deficient mice [39].

The PET-CT studies have also demonstrated differences between tissues in the rate of copper clearance. This could be due to the presence (and potential change in the expression/activity) of the second copper–efflux system, *Atp7a*. For example, the efflux of copper from kidneys is expected to be decreased by *Atp7b* gene knock-out; however, our data revealed faster initial rate of copper efflux from *Atp7b*$^{-/-}$ kidneys compared to control. This could be due to a significant change in the intracellular localization of Atp7a. Normally, in renal tubules ATP7A is located intra-cellularly, however in *Atp7b*$^{-/-}$ mice it is redistributed towards the basolateral membrane consistent with the role in copper efflux [40]. And yet, with age copper begins to accumulate in kidneys and in old *Atp7b*$^{-/-}$ mice (>9 months) renal copper is higher than in control [41], illustrating insufficiency of compensatory mechanisms. Overall, tissue-specific responses to copper deficiency and copper overload are well known [42–44], but the molecular mechanism behind tissue-specific responses to changing copper remains largely unexplored. The ability to measure the kinetics of copper distribution between tissues in real-time may greatly aid to understanding of such responses and have important implication for better tuning of copper supplement or chelating therapies.

Multiple positron emitting copper isotopes are available for tracking copper flow *in vivo* with PET, which include ^{60}Cu ($t_{1/2}$ 23.7 min, 93% β^+, 7% EC), ^{61}Cu ($t_{1/2}$ 3.32 h, 60% β^+, 40% EC), ^{62}Cu ($t_{1/2}$ 9.74 m; 98% β^+, 2% EC), and ^{64}Cu ($t_{1/2}$ 12.7 h, 17.4% β^+, 43% EC, 39% β^-). ^{64}Cu in the form of $^{64}CuCl_2$ can be potentially used as a simple tracer to assess copper metabolism in humans because (1) its relatively long half-life ($t_{1/2}$ 12.7 h) is desirable for tracking copper flow *in vivo* with PET; (2) it can be conveniently produced on a biomedical cyclotron and is commercially available in a ready-to-be-used chemical form ($^{64}CuCl_2$); and (3) $^{64}CuCl_2$ was used for assessing copper metabolism in the normal human subjects and the patients diagnosed with WD [29, 30, 32, 33]. Because of the 39% β^- emission from ^{64}Cu, it is essential to determine radiation dosimetry of $^{64}CuCl_2$ to ensure the safety of its use in humans. Based on a method used in the previous study in humans [29], we diluted $^{64}CuCl_2$ in 0.1 N HCl with saline containing 0.9% sodium chloride for intravenous administration of this tracer to the mice. Following intravenous administration, it is expected that $^{64}CuCl_2$ will immediately interact with abundant copper-binding proteins or molecules present in the plasma and cellular components of the blood. Absorption and distribution of ^{64}Cu in a specific organ or tissue will be governed by a sophisticated regulation mechanism related to perfusion of the organ or tissue and functional activity of the copper transporters and chaperons in the cells or tissues. Although copper handling machinery is highly conserved between human and rodents, the copper-carrying proteins are not identical and the difference in regulation and metabolic needs of copper by various organs exists in different species. The data from this study might be subject to errors, considering difference of copper metabolism among different species of animals. Given the fact that ^{64}Cu(II) in the form of $^{64}CuCl_2$ is easily accessible by other copper-transporting molecules *in vivo* after its injection, we regard $^{64}CuCl_2$ as an ideal source of ^{64}Cu(II) for tracking copper metabolism *in vivo*. On the other hand, we recognize that additional studies are needed to compare $^{64}CuCl_2$ with ^{64}Cu compounds in other chemical forms such as ^{64}Cu-citrate and ^{64}Cu-labeled human albumin to determine their roles in PET studies of copper metabolism in humans. Nevertheless, the data from this study has provided useful insights for further investigations of copper metabolism in humans using the noninvasive imaging technique of PET.

Based on its biodistribution in C57BL wild-type mice, human radiation dosimetry estimates of $^{64}CuCl_2$ were calculated to determine a safe dose for direct radiation dosimetry in

humans. Radiation dose to gallbladder was not calculated because of poor anatomic localization of gall-bladder on the CT images of the mice. The results of this preclinical study predict a radiation dose of $^{64}CuCl_2$ comparable to that of [^{18}F]FDG, when 5 MBq/kg (0.14 mCi/kg) of $^{64}CuCl_2$ is administered for PET in normal human subjects. Human dosimetry estimates obtained in our study may allow injection of 5 MBq/kg or 0.14 mCi/kg of $^{64}CuCl_2$ (350 MBq or 9.8 mCi of $^{64}CuCl_2$ for a 70-kg adult) for clinical PET scan in a normal human subject. However, in order to comply with the Code of Federal Regulation which limits the dose to the critical organ for a single study to 5 rem, a reduced tracer dose of 4 MBq/kg or 0.11 mCi/kg of $^{64}CuCl_2$ (280 MBq or 7.8 mCi of $^{64}CuCl_2$ for a 70-kg adult) may be used for PET imaging of copper metabolism in patients diagnosed with or suspected for WD. This needs to be adjusted following direct radiation dosimetry of $^{64}CuCl_2$ in humans. Because the amount of copper ions in a tracer dose of $^{64}CuCl_2$ is very small compared with the amount of copper (0.3–0.8 mg/d) absorbed from a normal diet [44], we do not expect significant toxicity or side effects from copper ions contained in a tracer dose of $^{64}CuCl_2$ for PET in humans.

Genetic testing alone is insufficient for predicting the severity and course of WD, as patients with identical mutations may show markedly different phenotype. The described methodology may find useful application in real-time assessing of copper metabolism misbalance in the patients with WD and other copper metabolic disorders such as Menkes disease caused by mutation of the *Atp7a* gene [10–12]. In addition, PET using $^{64}CuCl_2$ as a tracer is expected to be helpful for clinical management of the patients with WD by monitoring patient's response to copper-lowering therapy with penicillamine or other medications. Lastly, copper distribution in patients with neurological and hepatic manifestations can be measured and compared, which may contribute to better understanding of the diversity of phenotypic manifestations in WD.

Copper is required for cell proliferation and tumor angiogenesis [15]. Biodistribution of ^{64}Cu radioactivity was found to be different from that of [^{18}F]FDG, a glucose analog clinically used for imaging glucose metabolism, which was cleared from body mainly through renal clearance pathway, not through hepatobilliary clearance pathway [45]. PET using $^{64}CuCl_2$ may be used for localization and assessment of tumors located in a region where use of [^{18}F]FDG PET is limited by physiological background activity of [^{18}F]FDG. Because copper is required for tumor growth and angiogenesis, copper-chelating drugs such as tetrathiomolybdate (TM) were tested for anticancer therapy in a phase I clinical trial [46]. It was reported that different types of tumors had variable responses to TM treatment although molecular mechanisms for the difference in treatment response were not clear. We have previously demonstrated that human prostate cancer xenografts with increased uptake of $^{64}CuCl_2$ in mice could be visualized on the PET images [25]. Using $^{64}CuCl_2$ as a tracer, PET may be used to assess status of copper metabolism of the tumors and select the patients with tumors hypermetabolic in copper metabolism for personalized copper-lowering anticancer therapy.

Acknowledgments

The authors thank Jon Anderson and Anjali Gupta for technical support in calibration of PET-CT scanner and PET-CT scanning, and Guiyang Hao for help in tracer injection. This project was funded partially by National Institutes of Health, USA (R21EB005331-01A2 to F.P; R56DK084510 to SL) and the Department of Radiology and Harold C. Simmons Comprehensive Cancer Center, at University of Texas Southwestern Medical Center at Dallas, TX, USA. The production of Cu-64 at Washington University School of Medicine is supported by NCI grant R24 CA86307.

References

1. Olivares M, Uauy R. Copper as an essential nutrient. Am J Clin Nutr. 1996; 63(5):791S–6S. [PubMed: 8615366]
2. Uauy R, Olivares M, Gonzalez M. Essentiality of copper in humans. Am J Clin Nutr. 1998; 67(5 Suppl):952S–959S. [PubMed: 9587135]
3. Cartwright GE, Wintrobe MM. Copper metabolism in normal subjects. Am J Clin Nutr. 1964; 14:224–32. [PubMed: 14142382]
4. Turnlund JR. Human whole-body copper metabolism. Am J Clin Nutr. 1998; 67(5):960S–964S. [PubMed: 9587136]
5. Puig S, Thiele DJ. Molecular mechanisms of copper uptake and distribution. Curr Opin Chem Biol. 2002; 6:171–180. [PubMed: 12039001]
6. Lutsenko S. Human copper homeostasis: a network of interconnected pathways. Curr Opin Chem Biol. 2010; 14:1–7. [PubMed: 20022288]
7. Mercer JF. The molecular basis of copper-transport diseases. Trends Mol Med. 2001; 7:64–69. [PubMed: 11286757]
8. Bull PC, Thomas GR, Rommens JM, Forbes JR, Cox DW. The Wilson disease gene is a putative copper transporting P-type ATPase similar to the Menkes gene. Nat Genet. 1993; 5:327–337. [PubMed: 8298639]
9. Tanzi RE, Petrukhin K, Chernov I, Pellequer JL, Wasco W, Ross B, et al. The Wilson disease gene is a copper transporting ATPase with homology to the Menkes disease gene. Nat Genet. 1993; 5:344–350. [PubMed: 8298641]
10. Vulpe C, Levinson B, Whitney S, Packman S, Gitschier J. Isolation of a candidate gene for Menkes disease and evidence that it encodes a copper-transporting. Nat Genet. 1993; 3:7–13. [PubMed: 8490659]
11. Mercer JF, Livingston J, Hall B, Paynter JA, Begy C, Chandrasekhar-appa S, et al. Isolation of a partial candidate gene for Menkes disease by positional cloning. Nat Genet. 1993; 3:20–25. [PubMed: 8490647]
12. Chelly J, Tumer Z, Tonnesen T, Petterson A, Ishikawa-Brush Y, Tommerup N, et al. Isolation of a candidate gene for Menkes disease that encodes a potential heavy metal binding protein. Nat Genet. 1993; 3:14–19. [PubMed: 8490646]
13. Olivarez L, Caggana M, Pass KA, Ferguson P, Brewer GJ. Estimate of the frequency of Wilson's disease in the US Caucasian population: a mutation analysis approach. Ann Hum Genet. 2001; 65:459–463. [PubMed: 11806854]
14. Multhaup G. Amyloid precursor protein, copper and Alzheimer's disease. Biomed Pharmacother. 1997; 51(3):105–11. [PubMed: 9181045]
15. Theophanides T, Anastassopoulou J. Copper and carcinogenesis. Crit Rev Oncol Hematol. 2002; 1:57–64. [PubMed: 11923068]
16. Kusleikaite M, Masironi R. Trace elements in prognosis of myocardial infarction and sudden coronary death. J Trace Elem Exp Med. 1996; 9(2):57–62.
17. Owen CA Jr. Distribution of copper in the rat. Am J Physiol. 1964; 207:446–448. [PubMed: 14205364]
18. Owen CA Jr. Metabolism of radiocopper (Cu64) in the rat. Am J Physiol. 1965; 209:900–904. [PubMed: 5849489]
19. Dunn MA, Green MH, Leach RM Jr. Kinetics of copper metabolism in rats: a compartmental model. Am J Physiol. 1991; 261:E115–125. [PubMed: 1858867]
20. Que EL, Chang CJ. A smart magnetic resonance contrast agent for selective copper sensing. J Am Chem Soc. 2006; 128:15942–15943. [PubMed: 17165700]
21. Que EL, Gianolio E, Baker SL, Wong AP, Aime S, Chang CJ. Copper-responsive magnetic resonance imaging contrast agents. J Am Chem Soc. 2009; 131(24):8527–8536. [PubMed: 19489557]
22. Chaudhry AF, Verma M, Morgan MT, Henary MM, Siegel N, Hales JM, et al. Kinetically controlled photoinduced electron transfer switching in Cu(I)-responsive fluorescent probes. J Am Chem Soc. 2010; 132 (2):737–747. [PubMed: 20020716]

23. Domaille DW, Zeng L, Chang CJ. Visualizing ascorbate-triggered release of labile copper within living cells using a ratiometric fluorescent sensor. J Am Chem Soc. 2010; 132(4):1194–1195. [PubMed: 20052977]
24. Blower PJ, Lewis JS, Zweit J. Copper radionuclides and radiopharmaceuticals in nuclear medicine. Nucl Med Biol. 1996; 23:957–980. [PubMed: 9004284]
25. Peng F, Xin Lu, Janisse J, Muzik O, Shields AF. Positron emission tomography of human prostate cancer xenografts in mice with increased uptake of copper (II)-64 chloride. J Nucl Med. 2006; 47(10):1649–1652. [PubMed: 17015901]
26. Liu J, Hajibeigi A, Ren G, Lin M, Siyambalapitiyage W, Liu Z, et al. Retention of the radiotracers 64Cu-ATSM and 64Cu-PTSM in human and murine tumors is influenced by MDR1 protein expression. J Nucl Med. 2009; 50:1332–1339. [PubMed: 19617332]
27. Stabin MG. MIRDOSE: personal computer software for internal dose assessment in nuclear medicine. J Nucl Med. 1996; 37:538–46. [PubMed: 8772664]
28. Stabin MB, Siegel JA. Physical models and dose factors for use in internal dose assessment. Health Phys. 2003; 85:294–310. [PubMed: 12938720]
29. Osborn SB, Szaz KF, Walshe JM. Studies with radioactive copper (64Cu and 67Cu): abdominal scintiscans in patients with Wilson's disease. Q J Med. 1969; 38:467–474. [PubMed: 5355538]
30. Walshe JM, Potter G. The pattern of the whole body distribution of radioactive copper (67Cu, 64Cu) in Wilson's disease and various control groups. Q J Med. 1977; 46:445–462. [PubMed: 413153]
31. Hays MT, Watson EE, Thomas SR, Stabin. Radiation absorbed dose estimates from 18 F-FDG. J Nucl Med. 2002; 43:210–214. [PubMed: 11850487]
32. Bush JA, Mahoney JP, Markowitz H, Gubler CJ, Cartwright GE, Wintrobe MM. Studies on copper metabolism. XVI. Radioactive copper studies in normal subjects and in patients with hepatolenticular degeneration. J Clin Invest. 1955; 34:1766–1778. [PubMed: 13271562]
33. Skromne-Kadlubik G, Diaz JF, Celis C. Basal ganglia scans in the human. J Nucl Med. 1975; 16(8):787–788. [PubMed: 1177052]
34. Bissig KD, Honer M, Zimmermann K, Summer KH, Solioz M. Whole animal copper flux assessed by positron emission tomography in the Long–Evans cinnamon rat—a feasibility study. Biometals. 2005; 18(1):83–88. [PubMed: 15865413]
35. Wahl RL, Quint LE, Cieslak RD, Aisen AM, Koeppe RA, Meyer CR. Anatometabolic tumor imaging: fusion of FDG PET with CT or MRI to localize foci of increased activity. J Nucl Med. 1993; 34:1190–1197. [PubMed: 8315501]
36. Judenhofer MS, Wehrl HF, Newport DF, Catana C, Siegel SB, Becker M, et al. Simultaneous PET-MRI: a new approach for functional and morphological imaging. Nat Med. 2008; 14(4):459–465. [PubMed: 18376410]
37. Huster D, Finegold MJ, Morgan CT, Burkhead JL, Nixon R, Vanderwerf SM, Gilliam CT, Lutsenko S. Consequences of copper accumulation in the livers of the *Atp7b-/-*(Wilson disease gene) knockout mice. Am J Pathol. 2006; 168(2):423–434. [PubMed: 16436657]
38. Lee SH, Lancey R, Montaser A, Madani N, Linder MC. Ceruloplasmin and copper transport during the latter part of gestation in the rat. Proc Soc Exp Biol Med. 1993; 203(4):428–39. [PubMed: 8394586]
39. Harris ZL, Durley AP, Man TK, Gitlin JD. Targeted gene disruption reveals an essential role for ceruloplasmin in cellular iron efflux. Proc Natl Acad Sci USA. 1999; 96(19):10812–10817. [PubMed: 10485908]
40. Linz R, Barnes NL, Zimnicka AM, Kaplan JH, Eipper B, Lutsenko S. The intracellular targeting of copper-transporting ATPase ATP7A in a normal and *ATP7b*$^{-/-}$ kidney. Am J Physiol Renal Electrolyte Physiol. 2008; 294(1):F53–61.
41. Buiakova OI, Xu J, Lutsenko S, Zeitlin S, Das K, Das S, Ross BM, Mekios C, Scheinberg IH, Gilliam TC. Null mutation of the murine *ATP7B* (Wilson disease) gene results in intracellular copper accumulation and late-onset hepatic nodular transformation. Hum Mol Genet. 1999; 8(9): 1665–71. [PubMed: 10441329]
42. Li Y, Wang L, Schuschke DA, Zhou Z, Saari JT, Kang YJ. Marginal dietary copper restriction induces cardiomyopathy in rats. J Nutr. 2005; 135(9):2130–2136. [PubMed: 16140888]

43. Juhasz-Pocsine K, Rudnicki SA, Archer RL, Harik SI. Neurologic complications of gastric bypass surgery for morbid obesity. Neurology. 2007; 68(21):1843–1850. [PubMed: 17515548]

44. Turnlund JR, KeyesWR EHL, Acord LL. Copper absorption and retention in young men at three levels of dietary copper using the stable isotope ^{65}Cu. Am J Clin Nutr. 1989; 49:870–878. [PubMed: 2718922]

45. Fueger BJ, Czernin J, Hildebrandt I, Tran C, Halpern BS, Stout D, et al. Impact of animal handling on the results of 18 F-FDG PET studies in mice. J Nucl Med. 2006; 47:999–1006. [PubMed: 16741310]

46. Brewer GJ, Dick RD, Grover DK, LeClaire V, Tseng M, Wicha M, et al. Treatment of metastatic cancer with tetrathiomolybdate, an anticopper, antiangiogenic agent: phase I study. Clin Cancer Res. 2000; 6:1–10. [PubMed: 10656425]

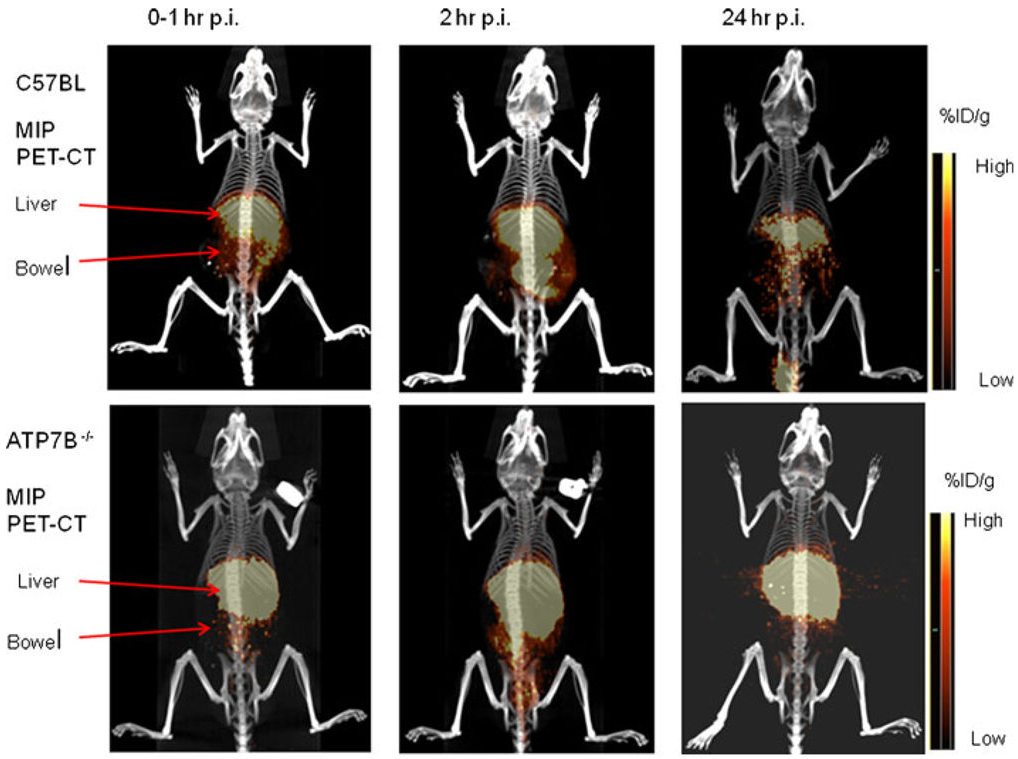

Fig. 1.

Representative PET-CT images of *Atp7b*$^{-/-}$ mice injected with $^{64}CuCl_2$ intravenously. Whole body PET-CT images of an *Atp7b*$^{-/-}$ mouse and a wild-type C57BL mouse were obtained during the first hour by dynamic imaging (0–1 h), and static at 2 and 24 h post-injection (p.i.) of $^{64}CuCl_2$, respectively. On the images obtained during the first hour post-injection, intense ^{64}Cu radioactivity was seen in the liver of *Atp7b*$^{-/-}$ and wild-type mice, with much less radioactivity in the muscle and brain. Diffuse radioactivity in the abdomen represents ^{64}Cu radioactivity in the intestinal tracts resulted from hepatobilliary clearance. At 2 and 24 h post-injection, intense ^{64}Cu radioactivity remained in the liver of *Atp7b*$^{-/-}$ mouse, in contrast to reduced ^{64}Cu radioactivity in the liver of wild-type C57BL mice. There is little ^{64}Cu radioactivity in the urinary bladder, which indicates that ^{64}Cu is mainly cleared through hepatobilliary clearance pathway. MIP (maximum intensity projection), *Scale bar* %ID/g (percentage of injected dose per gram).

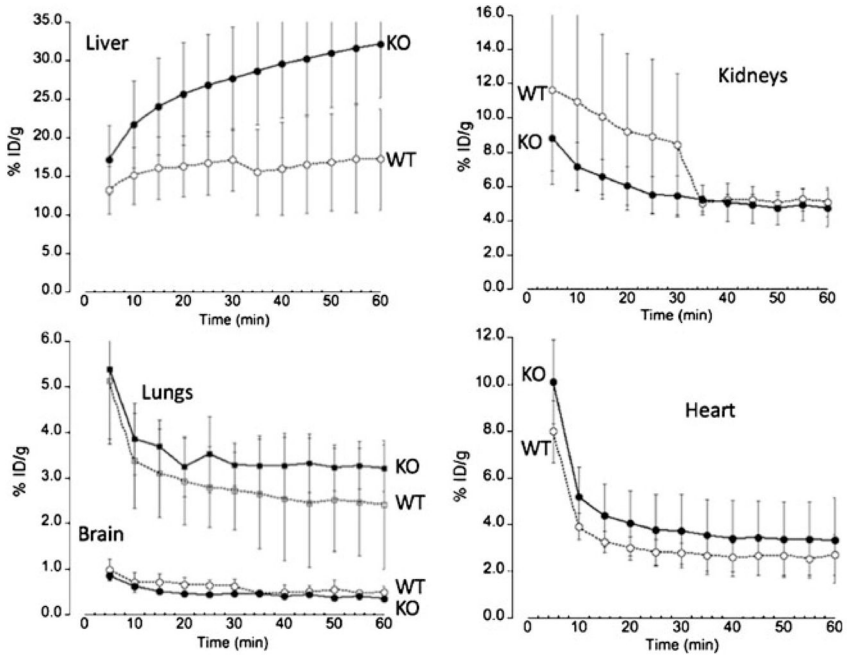

Fig. 2.

Time-activity plots of ^{64}Cu radioactivity distribution in the mice post intravenous injection with $^{64}CuCl_2$. Decay corrected time–activity curves were obtained from average of ^{64}Cu radioactivity at various time points (minutes) post intravenous injection of $^{64}CuCl_2$ in mice [KO, *ATP7b*$^{-/-}$ knock-out mice (*N*=4) and WT, wild type C57BL mice (*N*=4)]. Hepatic uptake of ^{64}Cu in the *Atp7b*$^{-/-}$ mice is higher than that by the control C57BL mice, with continuing accumulation of ^{64}Cu in the *Atp7b*$^{-/-}$ mice. Following rapid decrease of ^{64}Cu radioactivity from blood pool, tracer concentrations in the lungs and heart are stable, with relatively low tracer uptake in the brain in the *Atp7b*$^{-/-}$ and control C57BL mice. Initial renal uptake of ^{64}Cu in the control C57BL mice is higher than that in the *ATP7b*$^{-/-}$ mice. Subsequently, ^{64}Cu radioactivity in the kidneys of the control C57BL mice has gradually decreased to the similar level in the *ATP7b*$^{-/-}$ mice.

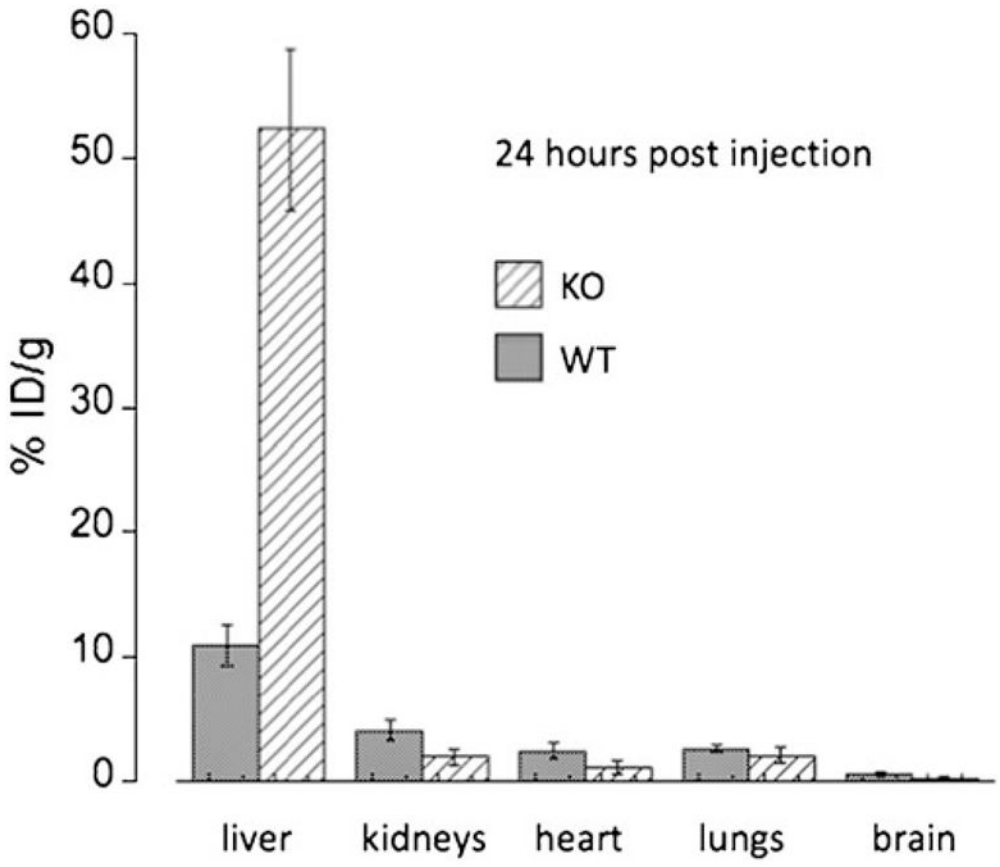

Fig. 3.

Comparison of the %ID/g at 24 h post-injection in several organs of *Atp7b*$^{-/-}$ knock-out (KO) and C57BL wild-type (WT) mice. In the liver, the %ID/g of KO mice was significantly higher than that in the WT mice, whereas in all other organs the %ID/g was significantly lower in the KO mice, except for the lungs where the difference was not significant (see text).

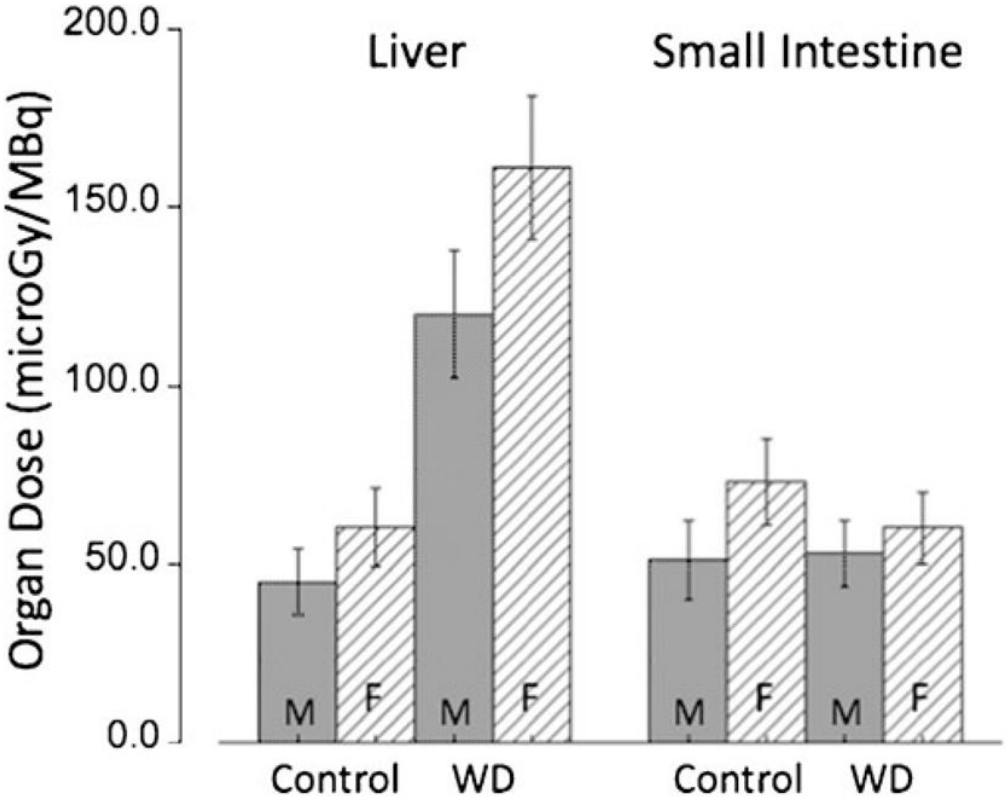

Fig. 4.

Organ doses (μGy/MBq) to the critical organs in control subjects (small intestine) and to patients with WD (liver). Doses for females are higher than those for males. *Error bars* indicate the standard deviation (SD) for *N*=4 independent experiments.

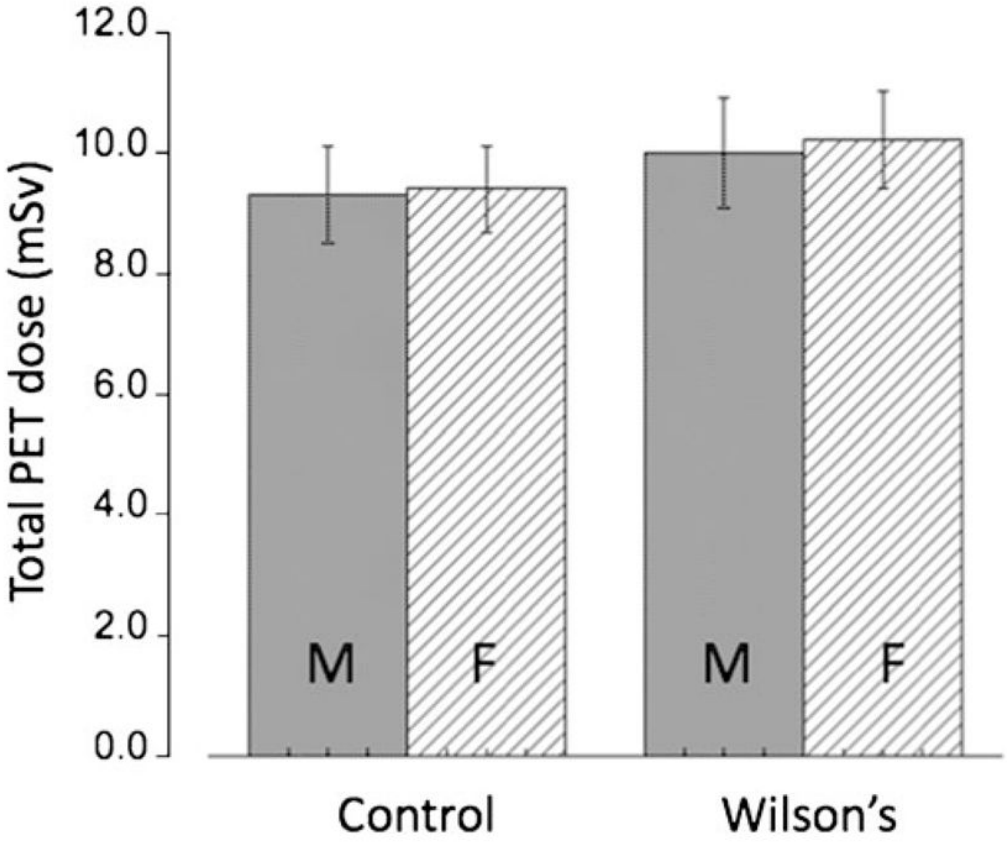

Fig. 5.

Total PET dose from a $^{64}CuCl_2$ PET scan in both genders for control subjects and patients with WD (injected activity 5 MBq/kg). The doses for females are higher than those for males. *Error bars* indicate the standard deviation (SD) for *N*=4 independent experiments.

Table 1

Mean residence times (hours) and corresponding standard deviation for $^{64}CuCl_2$ obtained from PET imaging in control (C57BL) and *Atp7b*$^{-/-}$ mice

	C57BL	***Atp7b*$^{-/-}$**
Blood	0.384±0.216	0.288±0.108
Brain	0.028±0.015	0.016±0.007
Heart	0.022±0.010	0.029±0.011
Lungs	0.081±0.027	0.129±0.013
Liver	0.821±0.257	2.448±0.315
Small bowel	0.348±0.257	0.283±0.081
Upper large bowel	0.115±0.073	0.020±0.001
Lower large bowel	0.024±0.012	0.011±0.005
Kidneys	0.064±0.024	0.057±0.010
Bladder	0.021±0.005	0.027±0.010
Muscle	0.685±0.326	0.504±0.183
Testes	0.0012±0.0001	0.0014±0.0001

Table 2

Radiation absorbed dose estimates for $^{64}CuCl_2$ in adult control subjects and patients with WD

	Dose (μGy/MBq)			
Target	**Control**		**Wilson's disease**	
Organ	**Adults male**	**Adult female**	**Adults male**	**Adult female**
Adrenals	27.0±1.3	35.1±0.1	28.8±1.3	36.4±0.1
Brain	5.9±1.1	7.5±1.0	4.7±1.3	6.2±0.1
Breast	–	30.0±0.2	–	27.8±0.1
Gallbladder wall	29.0±14	37.4±8.9	33.7±1.3	40.8±0.1
LL intestine	34.0±8.9	42.1±0.5	28.2±1.3	35.3±0.1
Small intestine	60.5±12	69.0±0.5	52.7±1.3	60.1±0.1
Stomach	27.2±2.6	35.6±0.3	26.8±1.3	33.6±0.1
UL intestine	48.6±1.2	58.1±0.7	31.3±1.3	38.7±0.1
Heart wall	15.4±1.3	19.8±1.0	18.5±1.3	23.6±0.1
Kidneys	26.0±2.2	30.1±7.0	26.0±1.3	29.6±0.1
Liver	44.4±12	59.6±4.2	120.0±1.3	161.0±1.7
Lungs	14.0±1.1	19.8±0.6	18.9±1.3	23.9±0.1
Muscle	10.3±1.2	13.8±0.1	10.2±1.3	13.2±0.1
Ovaries	–	36.8±1.2	–	32.8±0.1
Pancreas	28.3±1.2	37.2±0.2	29.4±1.3	36.2±0.1
Red Marrow	21.6±2.8	27.7±0.4	21.1±1.3	25.7±0.1
Osteogenic cells	50.2±2.6	67.5±1.8	47.4±1.3	62.8±0.1
Skin	21.0±1.1	27.6±0.1	20.0±1.3	25.3±0.1
Spleen	26.4±1.4	34.6±0.2	25.4±1.3	32.0±0.1
Testes	9.1±2.2	–	8.6±1.3	–
Thymus	24.4±2.4	32.9±0.2	23.5±1.3	30.4±0.1
Thyroid	24.2±2.2	31.1±0.2	22.8±1.3	28.2±0.1
Urinary Bladder wall	29.6±2.5	33.3±4.1	28.8±1.3	32.7±0.1
Uterus	–	36.1±0.4	–	32.9±0.1
Total body	26.4±1.4	34.8±0.2	26.8±1.3	34.4±0.1

LL intestine lower large intestine, *UL intestine* upper large intestine

Table 3

Radiation absorbed dose from $^{64}CuCl_2$ PET studies in control subjects and patients with WD

Subjects	Effective Dose (ED) μSv/MBq (rem/mCi)	Critical Organ μGy/MBq (rad/mCi)	Effect PET dose[a] mSv (rem)
Control male (70 kg)	26.5 (0.098)	50.2 (0.187)[b]	9.3 (0.96)
Control female (57 kg)	32.8 (0.121)	73.4 (0.271)[b]	9.4 (0.97)
WD male (70 kg)	28.6 (0.105)	120 (0.445)[c]	10.0 (1.03)
WD female (57 kg)	35.7 (0.132)	161 (0.594)[c]	10.2 (1.05)

[a] Injected activity of 5 MBq/kg (0.14 mCi/kg)

[b] Small intestines

[c] Liver